Crossover from type I to type II regime of mesoscopic superconductors of the first group

Leonardo Rodrigues Cadorim[1], **Thiago de Oliveira Calsolari**[1], **Rafael Zadorosny**[2], **Edson Sardella**[2]

[1]Departamento de Física, Faculdade de Ciências, Universidade Estadual Paulista (UNESP), Caixa Postal 473, 17033-360, Bauru-SP, Brazil

[2]Departamento de Física e Química, Faculdade de Engenharia de Ilha Solteira, Universidade Estadual Paulista (UNESP), Caixa Postal 31, 15385-000 Ilha Solteira-SP, Brazil

E-mail: `edson.sardella@unesp.br`

July 2019

Abstract. In the present work, we have studied the crossover between type I and type II superconductivity on mesoscopic superconducting thin films by numerically solving the 3D Ginzburg-Landau equations. We determined the dependence on temperature of the critical Ginzburg-Landau parameter $\kappa_c(d)$, below which the superconductor behaves as type I for a given thickness d of the film. The effect of the sample dimensions on this crossover was also investigated. Additionally, we report a novel giant vortex configuration with a local minimum of the magnetic field at the centre of the core. Finally, we present certain results suggesting that the vortex-vortex interaction is not monotonic, varying instead from long-range attraction to short-range repulsion.

1. Introduction

The distinct magnetic properties of type I and type II bulk superconductors lie in the signal of the surface energy density, which is positive for the former and negative for the latter. The transition between these two types are given by the Ginzburg-Landau parameter κ, the superconductor being of type II when $\kappa > 1/\sqrt{2}$ and of type I if $\kappa < 1/\sqrt{2}$. The former is energetically favourable to the penetration of vortices; in the latter, the penetration of magnetic flux leads the superconductor to the normal state.

Tinkham [1] first showed, using an argument based on fluxoid quantization, that superconducting thin films, even of material with $\kappa < 1/\sqrt{2}$, can behave like type II if the film is sufficiently thin, possessing a second-order phase transition to the normal state. Pearl [2] showed that, unlike bulk superconductors, vortices in very thin films of type I have a long-range repulsion, thus making possible the formation of a vortex lattice. In an analysis similar to Abrikosov [3], Maki [4] mathematically proved Tinkham's hypothesis that a fluxoid structure is indeed a solution to the Ginzburg-Landau equations for a thin film of a type I superconductor, provided that the film is thinner than a certain critical thickness.

Later work by Lasher [5] and Callaway [6] extended Maki's analysis by considering other types of vortex structures, like the possibility of the formation of giant vortices. Lasher showed that, although very thin films do exhibit a triangular lattice, films of intermediate thickness possess a more complex structure, allowing for different patterns, including vortices with more than a quantum flux. He then predicted the existence of two critical thicknesses, one corresponding to the triangular lattice phase and a second, larger one delimiting the mixed and the intermediate states in the film.

Much numerical work has been carried out on these giant vortices configurations in superconducting thin films. For example, Schweigert *et al.* [7] studied the vortex phase diagrams on thin disks of various radii and thicknesses, finding the transition between the multivortex and giant vortex configurations. Similarly, Shi *et al.* [8] found the same transition while studying mesoscopic rings of variable radii. Berdiyorov *et al.* [9] analysed the vortex structures in thin films with an antidot array. By varying the effective Ginzburg-Landau parameter and the periodicity of the antidot lattice, they provided a structural phase diagram for such a system. Palonen *et al.* [10] performed simulations for low κ type I superconductors, finding that giant vortex configurations are stable in intermediate thickness films, but for sufficiently thin films only single vortex states are stable. They also speculated that the giant vortex formation is possible due to a short-range attraction and a long-range repulsion. Córdoba *et al.* [11] analysed the stability of the giant vortices, varying both the temperatures and thicknesses of the film. They found that the formation of those specimens is hindered by increases in temperature.

Dantas *et al.* [12] used a set of constrained Ginzburg-Landau equations to calculate the vortex-vortex interaction potential of a series of thin films of different thicknesses and κ values. They found that vortex-vortex interaction is non-monotonic; its behaviour depends on the film's thickness and κ. They then constructed a phase diagram delimiting the regions where the film showed a single fluxoid lattice, giant vortex configuration, and type I behaviour. With this phase diagram, they were able to find the critical κ value that makes possible the formation of a vortex lattice in thin films. The value they encountered is different from the $\kappa_{eff} = 2\kappa^2/d$ that is generally assumed for thin films.

The present study investigates the influence of temperature and the surface effects introduced by the mesoscopic dimensionality of the samples in the critical parameters of this well-known crossover from type I to type II superconductivity in superconducting thin films.

By numerically solving the 3D Ginzburg-Landau equations, we studied the temperature dependence of the crossover between type I and type II regimes for mesoscopic superconducting thin films. Type I superconducting mesoscopic samples were simulated, and an expression relating the Ginzburg-Landau parameter of the material to its critical thickness was obtained, above which the nucleation of vortices becomes possible for different temperatures. We then studied how the dimensions of the film that are perpendicular to the applied field influence the previously found expressions of critical thicknesses. We also analysed the structures of the vortex pattern and their respective evolution within two different regimes, the zero-field-cooled (ZFC) and the field-cooled (FC) procedures.

We add the following final introductory remark regarding terminology. By *type I regime*, we mean a superconductor in a vortex-free state for every value of the applied magnetic field until superconductivity is destroyed. We use *type II regime* to indicate a superconductor that nucleates one or more vortices before the destruction of superconductivity, even if the vortex-vortex interaction is not monotonically repulsive.

The outline of this paper is as follows. In Section 2, we present the theoretical formalism of the 3D Ginzburg-Landau equations and the numerical solution approaches that guided this work. In Section 3, we determine the critical parameters that define the crossover from a type I to a type II regime. Next, in Section 4 we demonstrate several vortex configurations, such as the single-vortex, giant-vortex, and multivortex states. Finally, we present concluding remarks in Section 5.

2. Theoretical Formalism

The system we investigate consists of a mesoscopic superconducting film of dimensions (l_x, l_y, l_z) inside a larger box (L_x, L_y, L_z) to take into account the effects of a stray magnetic field. The superconductor is immersed in a uniformly applied magnetic field $\mathbf{H}$ oriented along the z direction. The geometry of the system is illustrated in Fig. 1. We consider the dimensions of the domain Ω sufficiently large such that the local magnetic field equals an externally applied one $\mathbf{H}$ at the interface $\partial\Omega$.

Our starting point is the 3D time-dependent Ginzburg-Landau equations (TDGL for short) that describe the superconducting state. They are coupled partial differential equations, one for the order parameter ψ and another for the vector potential $\mathbf{A}$, which is related to the local magnetic field through the expression $\mathbf{h} = \boldsymbol{\nabla} \times \mathbf{A}$. In order to fulfil the experimental observation of the dependence of the critical thermodynamic field $H_c(T) \propto [1 - (T/T_c)^2]$, we have modified the GL equations according to [13], so they now read:

$$\begin{aligned} \frac{\partial\psi}{\partial t} &= -\left(-i\boldsymbol{\nabla} - \mathbf{A}\right)^2\psi \\ &\quad + \frac{1}{(1+\tau^2)^2}\psi(1 - \tau^4 - |\psi|^2)\ ,\ \text{in } \Omega_{sc}, \end{aligned} \tag{1}$$

$$\frac{\partial\mathbf{A}}{\partial t} = \begin{cases} \mathbf{J}_s - \kappa(0)^2\boldsymbol{\nabla}\times\boldsymbol{\nabla}\times\mathbf{A}\ ,\ \text{in } \Omega_{sc}, \\ -\kappa(0)^2\boldsymbol{\nabla}\times\boldsymbol{\nabla}\times\mathbf{A}\ , \quad \text{in } \Omega\backslash\Omega_{sc}, \end{cases} \tag{2}$$

where $\mathbf{J}_s = \mathrm{Re}\left[\bar{\psi}(-i\boldsymbol{\nabla} - \mathbf{A})\psi\right]$ is the superconducting current density. In order to ensure that the local magnetic field $\mathbf{h}$ equals the applied field $\mathbf{H}$ far away from the superconducting region Ω_{sc}, we take a sufficiently large domain Ω. We also demand that no superconducting current flows from the superconductor towards the vacuum, which means that the superconducting current density vanishes at the superconductor-vacuum

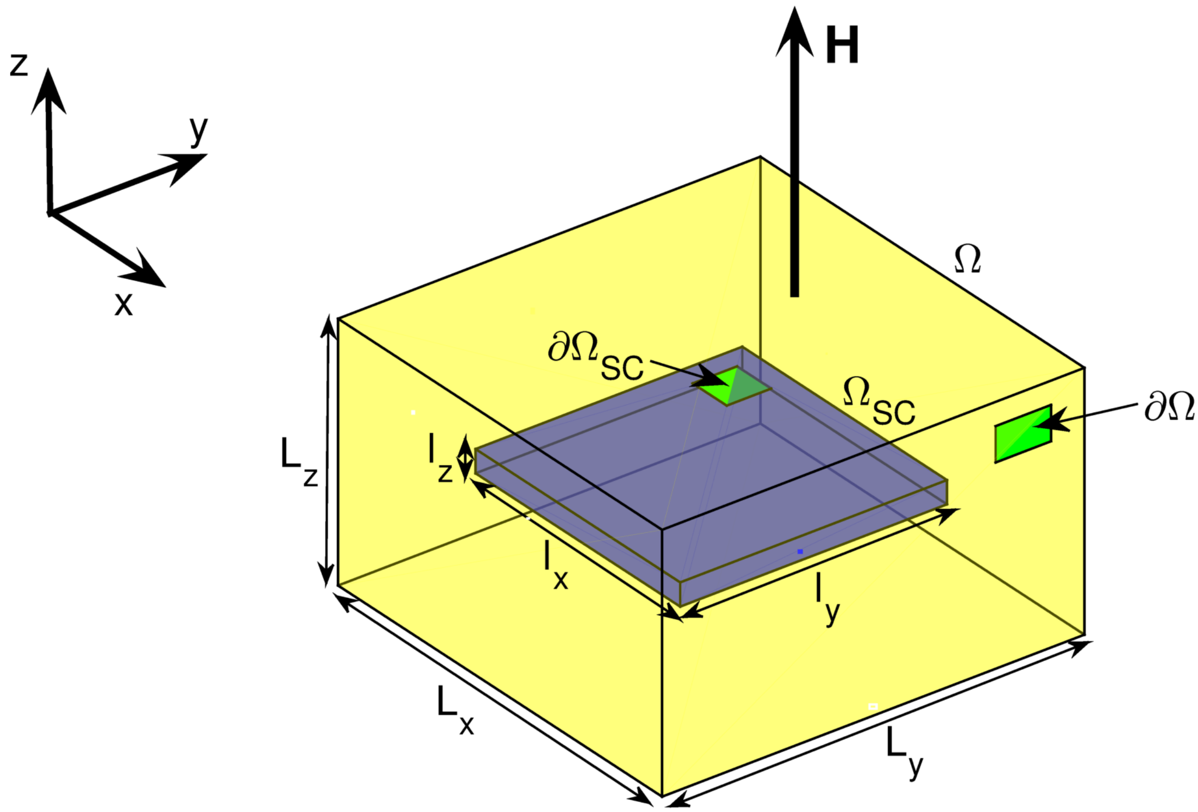

Figure 1. (Color online) Schematic view of the studied system.

boundary $\partial\Omega_{sc}$. Defining a unit vector normal to the superconductor-vacuum interface $\mathbf{n}$, this asserts that our equations 1 and 2 satisfy the following boundary conditions:

$$\mathbf{n} \cdot (i\boldsymbol{\nabla} + \boldsymbol{A})\psi = 0 \text{ , in } \partial\Omega_{sc}, \tag{3}$$

$$\boldsymbol{\nabla} \times \mathbf{A} = \mathbf{H} \text{ , in } \partial\Omega. \tag{4}$$

Here, the order parameter is in units of $\psi_\infty(0) = \sqrt{-\alpha(0)/\beta(0)}$ (the order parameter at the Meissner state), where $\alpha(\tau)$ and $\beta(\tau)$ are two phenomenological constants, $\tau \equiv T/T_c$ is the temperature T in units of the critical temperature T_c, lengths are in units of the coherence length $\xi(0)$, time is in units of the Ginzburg-Landau characteristic time $t_0 = \pi\hbar/8K_BT_c$, and the vector potential $\mathbf{A}$ is in units of $\xi(0)H_{c2}(0)$, where $H_{c2}(\tau)$ is the bulk upper critical field. In order to adjust the phenomenological constant to the thermodynamic critical field for type I superconductors, $H_c(\tau) = H_c(0)(1-\tau^2)$, the Ginzburg-Landau parameter becomes temperature dependent; we have $\kappa(\tau) = \xi(\tau)/\lambda(\tau) = \kappa(0)/(1+\tau^2)$, where $\lambda(\tau) = \lambda(0)/\sqrt{1-\tau^4}$ and $\xi(\tau) = \xi(0)\sqrt{(1+\tau^2)/(1-\tau^2)}$. The TDGL equations are used only as a relaxation method to achieve a stationary state. They were numerically solved by using the link-variable method (see, for instance, Refs. [14] and [15]), which was implemented in a GPU-accelerated forward-time-central-space scheme by using a mesh grid with no fewer than five points per $\lambda(\tau)$ and ten points per $\xi(\tau)$.

3. Critical Parameters

We studied mesoscopic superconducting thin films with a cross section of dimensions $12\xi(0) \times 12\xi(0)$ and variable thicknesses. In the numerical simulations, we used a box large enough to ensure that demagnetizing effects far away from the superconducting sample would become small. In all cases studied, the superconducting sample was initially set to be in the Meissner state and the applied magnetic field adiabatically increased in steps of $\Delta H = 10^{-3} H_{c2}(0)$ until superconductivity was destroyed (ZFC). For each value of the film thickness l_z, we varied the value of the Ginzburg-Landau parameter $\kappa(0)$ until we obtained the crossover between type I and type II behaviours for that specific $d \equiv l_z/\xi(0)$ value.

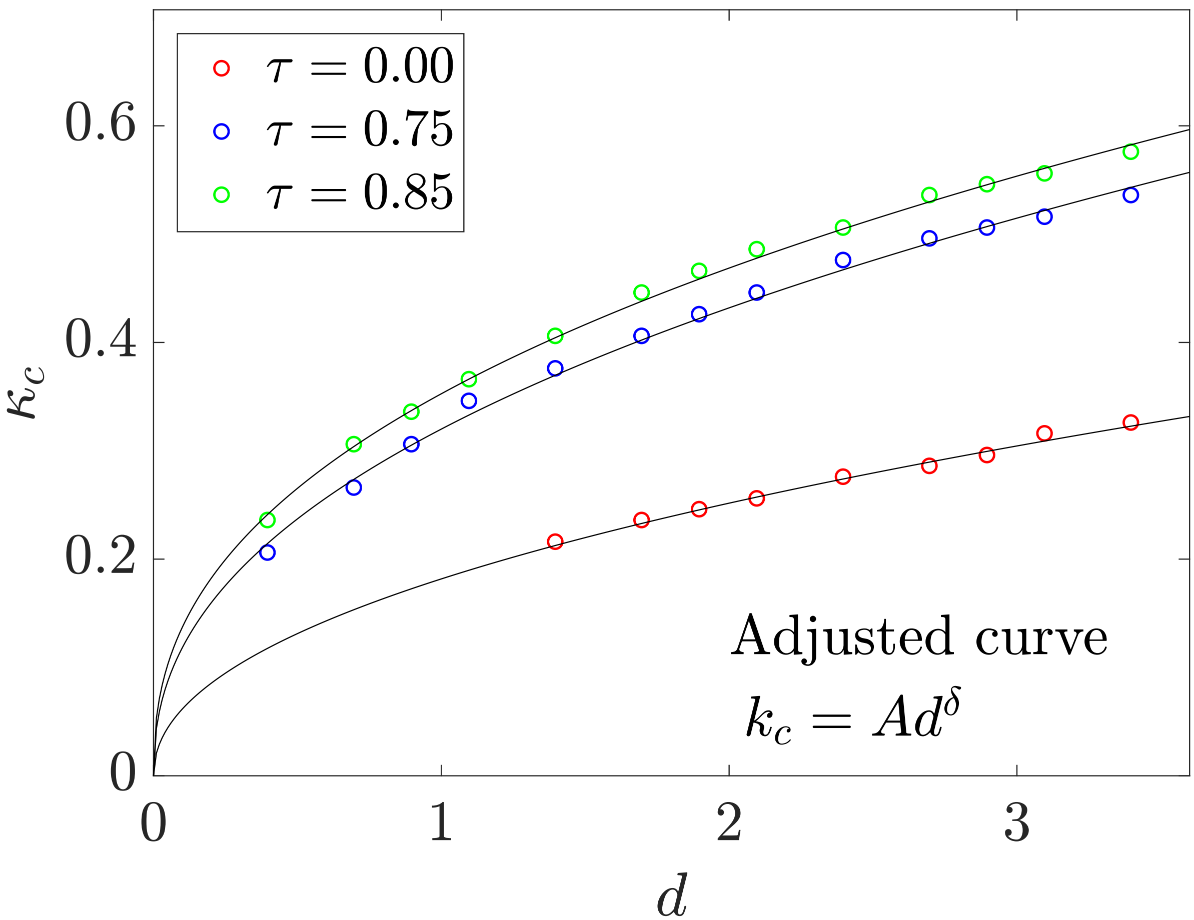

Figure 2. (Color online) Numerically obtained points and adjusted curves for the critical values of $\kappa(0)$ at three different temperatures for a superconductor with cross section $12\xi(0) \times 12\xi(0)$

Fig. 2 shows the expressions for the critical values of $\kappa(0)$, above which vortices are first seen, for three different temperatures $\tau = 0.00$, $\tau = 0.75$ and $\tau = 0.85$. Below this curve, the superconductor is type I; above the curve, it becomes type II. By fitting these curves with a function of the general form $\kappa_c = Ad^\delta$, we were able to find the values of the A and δ critical parameters. The respective forms of each curve are given by (a) $\kappa_c = 0.183d^{0.464}$, for $\tau = 0.00$, (b) $\kappa_c = 0.317d^{0.438}$, for $\tau = 0.75$, and (c) $\kappa_c = 0.351d^{0.416}$, for $\tau = 0.85$.

Contrary to previous studies concerning these critical parameters, we let the temperature remain entirely explicit so that we could determine the effect of temperature on the crossover from a type I to a type II regime.

As Fig. 2 shows, for a given value of the thickness d, the critical value of $\kappa(0)$ increases as the temperature rises. This behaviour can be explained by the fact that the transition from type I behaviour to the mixed state happens in an intertype phase [11, 16, 17], which, unlike both type I and conventional type II, has a non-monotonical vortex-vortex interaction. This transition between type I and intertype superconductivity happens for larger values of $\kappa(0)$ as the temperature approaches T_c [16], explaining our κ_c dependence on temperature.

To investigate the influence of the superconductor dimensions on the critical values, the same procedure was carried out on a sample of a cross section with dimensions $20\xi(0) \times 20\xi(0)$ and a variety of thicknesses. The temperature was set to $0.85T_c$. The resulting curve, presented in Fig. 3, was fit in the same way as the previous ones and was found to be $\kappa_c = 0.321d^{0.487}$.

As Fig. 3 shows, the critical κ_c for a superconductor of dimensions $20\xi(0)\times 20\xi(0)$ is below the analogous curve for the superconductor of size $12\xi(0)\times 12\xi(0)$. This behaviour could be explained by a competing effect between the vortex-vortex interactions and the vortex repulsion from the border of the sample directed towards the centre of the superconductor. This argument runs as follows. For a fixed value of $\kappa(0)$, the larger system presents a greater critical thickness than the smaller one. In these cases, the vortex-vortex interaction, although it may already be repulsive, cannot overcome the vortex exclusion from the barrier, which causes a considerable number of fluxoids to nucleate together at the centre in classic type I behaviour [5]. When the thickness of the sample is decreased to below d_c, the vortex-vortex repulsion due to the stray magnetic field is now able to suppress the border expulsion, nucleating a small number of fluxoids, which is a type II behaviour. If we carry out the same analysis on the smaller sample, we see that, due to their greater proximity, the vortices experience a more significant repulsion from the border, with a smaller thickness than the previous case being necessary for the vortex-vortex repulsion to overcome the border effect.

To corroborate this analysis, we studied the current distribution for both values of the sample dimension for a fixed $\kappa(0)$ and two thickness values, as shown in the red points of Fig. 3. In order to compare the two samples on an equal footing, we analysed their current distributions for values of the applied magnetic field, as shown by the red points in panel (a) of Fig. 4, for which the penetrated flux was the same for both samples. In panel (b), we show the intensity of the current at the border of the superconductor for both dimensions of the sample, with $\kappa(0) = 0.32$ and $d = 0.9$, in such a way that the smaller sample presents type I behaviour, while the larger one behaves as type II,

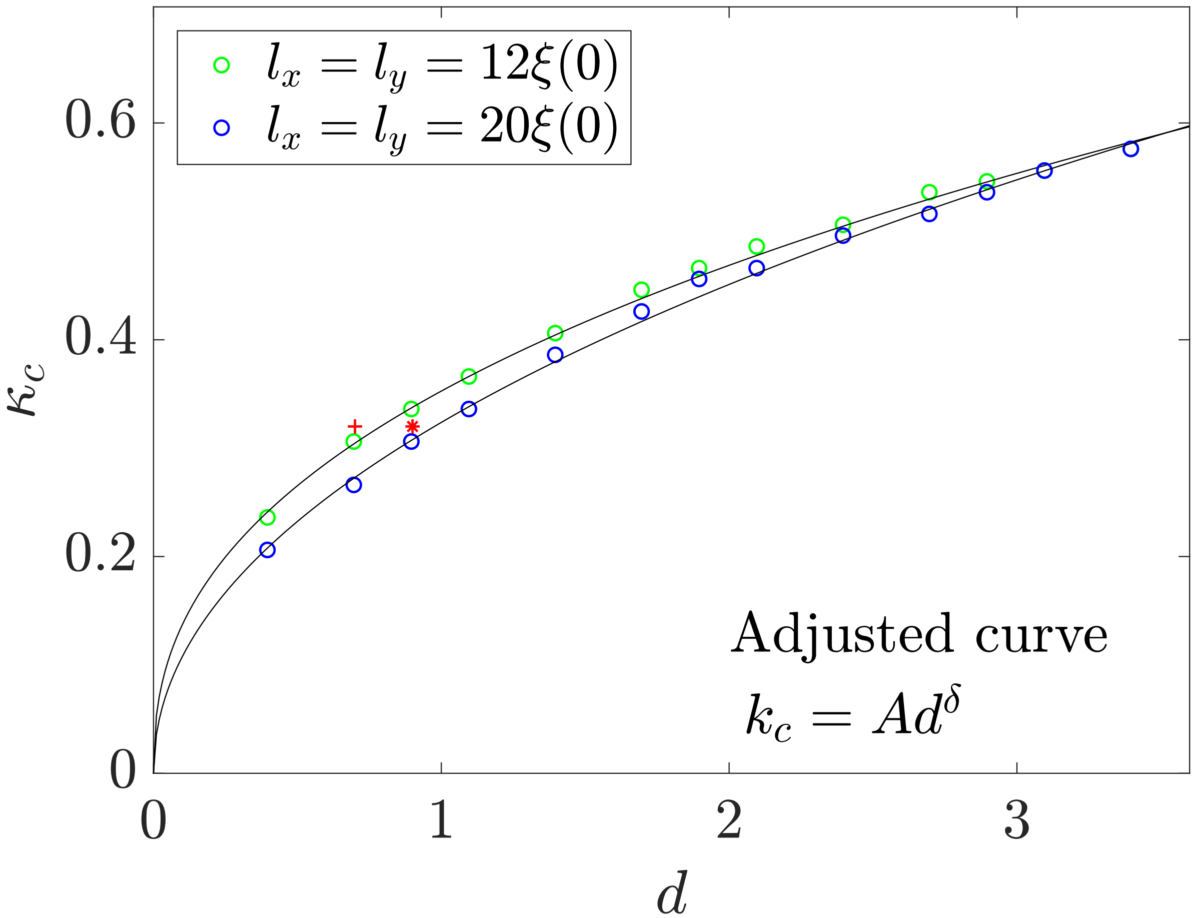

Figure 3. (Color online) Numerically obtained points and adjusted curves for the critical value of $\kappa(0)$ for the superconductor with two different cross sections. The temperature was fixed at $T = 0.85T_c$. The two points indicated in red are analysed in the text.

as shown in the magnetization curves in panel (a) of Fig. 4. ‡. As the figure shows, the currents are stronger for the smaller sample, giving support to our previous analysis. However, this does not mean that the $\kappa_c(d)$ curve will be monotonically lower for larger dimensions; at some point, the curve could go up, approaching the analytical predictions for infinite thin films [4, 5].

4. Vortex Configurations

We found the vortex configurations for both the ZFC and FC procedures; below, we present the results for both. For this, we fixed the temperature and took two different dimensions of the film.

‡ In panel (a) of Fig. 4, the jumps in the magnetization curve signal the entrance of one vortex or multiple vortices into the sample. The fact that the blue curve presents a single jump indicates that the system goes directly to the normal state, a type I behaviour, while the two jumps in the red curve indicate the presence of a vortex state before the transition to the normal state, a classic type II behaviour

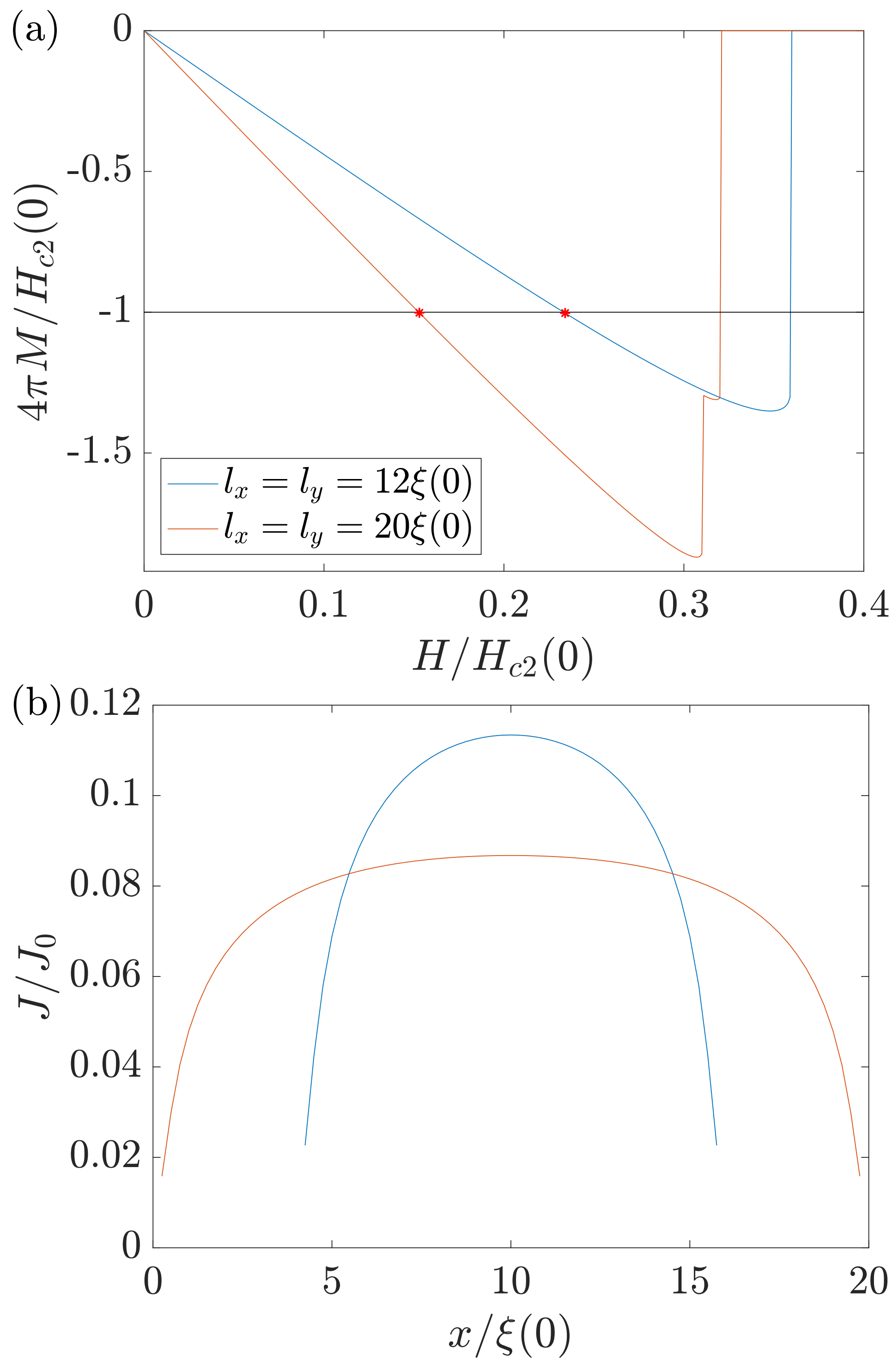

Figure 4. (Color online) (a) Magnetization curve for a sample with dimensions $l_x = l_y = 12\xi(0)$ (blue line) and $l_x = l_y = 20\xi(0)$ (red line). The red points indicate the values of the applied magnetic field for which both samples present equal magnetization. (b) The intensity of the currents on the border of the superconductor for a sample with dimensions $l_x = l_y = 12\xi(0)$ (blue line) and $l_x = l_y = 20\xi(0)$ (red line).

4.1. Zero-Field-Cooled

For the case $\kappa(0) = 0.40$ and different film thickness values, we followed the evolution of the vortex configurations as the applied magnetic field was increased from $H = 0$ in the Meissner state to the normal state (ZFC). For a system of dimensions $12\xi(0) \times 12\xi(0) \times 0.4\xi(0)$ and $\tau = 0.85$, a single vortex first nucleates and reaches equilibrium at the centre of the sample (see panel (a) of Fig. 5 for the magnitude of ψ). When the second vortex enters the superconductor, it collapses, with the existing one forming a giant vortex with vorticity $L = 2$, still at the centre of the sample (panel (b)). The same process recurs when the third vortex nucleates, now forming a giant vortex with vorticity $L = 3$ at the centre (panel (c)). As the fourth vortex enters, the existing giant vortex is broken apart, giving way to a configuration of four single vortices positioned at the vertices of a square around the centre of the sample (panel (d)). As the magnetic field gets even more intense, superconductivity is destroyed and the magnetic field is uniform everywhere.

For larger values of thickness d, at least up to $d = 0.60$, the system moves from the Meissner state directly to a giant vortex state with triple vorticity, after which it evolves in the same manner described above. We proceeded in the same manner for other values of $\kappa(0)$; similar configurations were obtained. All have a characteristic in common: namely, the maximum vorticity of the giant vortex state is $L = 3$. In addition, the first configuration just after the Meissner state consists of either a single or giant vortex.

The local magnetic field profiles corresponding to Fig. 5 are presented in Fig. 6, which shows the intensity of h_z in the xy plane. Our results exhibit a new scenario concerning the giant vortex state in type I superconducting films. It is well known that, at the centre of a vortex, the field has a local maximum, even for a giant vortex (see, for instance, Ref. [18]). As panel (a) shows, the field of a single vortex follows this general property. However, for the $L = 2$ giant vortex state (panel (b)), h_z has a local minimum at the centre. The flux is spread around the giant vortex core in the form of a ring. This is even more pronounced for the $L = 3$ giant vortex shown in panel (c). For the $L = 4$ single vortex state in panel (d), the magnetic field distribution shows a common pattern, exhibiting four local maxima. As H increases, the field becomes uniform everywhere.

In order to better visualize the evolution from the single vortex state (Fig. 6 panel (a)) to the giant vortex state with $L = 2$ (Fig. 6 panel (b)), we followed the transformation of the local magnetic field profile as the second vortex began to nucleate at the sample (see Fig. 7 panel (a)) until the two vortices coalesced at the centre of the sample at the equilibrium state. Fig. 7 shows some metastable vortex configurations for the applied magnetic field of $H = 0.247H_{c2}(0)$. Panels (b)-(d) show that, as the nucleating vortex moves towards the centre of the sample, both vortices suffer a deformation, combining themselves in a ring-like flux pattern (see panel (f)). Note the slight asymmetry in this last panel, which is due to the fact that it is still a metastable configuration but close to the stationary state of panel (b) in Fig. 6.

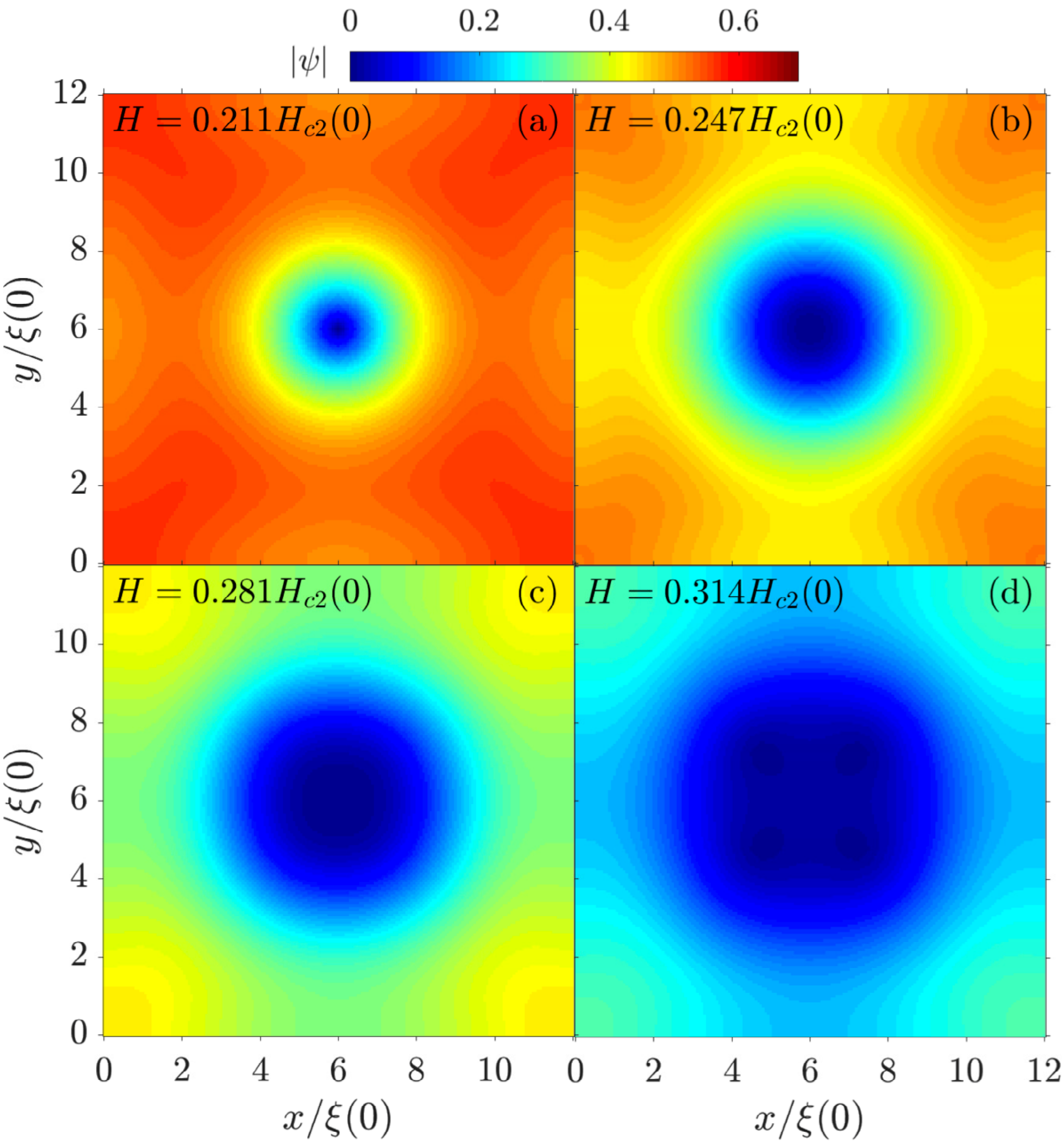

Figure 5. (Color online) Magnitude of the order parameter for four different values of applied magnetic field in the case of a superconducting thin film of dimensions $12\xi(0) \times 12\xi(0) \times 0.4\xi(0)$, $\kappa(0) = 0.40$ and $T = 0.85T_c$.

For larger thicknesses up to $d_c \sim 1.4$ we found only the $L = 4$ state of individual vortices similar to panel (d) of Fig. 6. Above this value of d, the system goes to a type I regime (see Fig. 2). By studying the dependence of the penetration field H_p on temperature, we found that, in accordance with previous experimental results [19], the field at which a vortex is first nucleated increases with decreasing temperature.

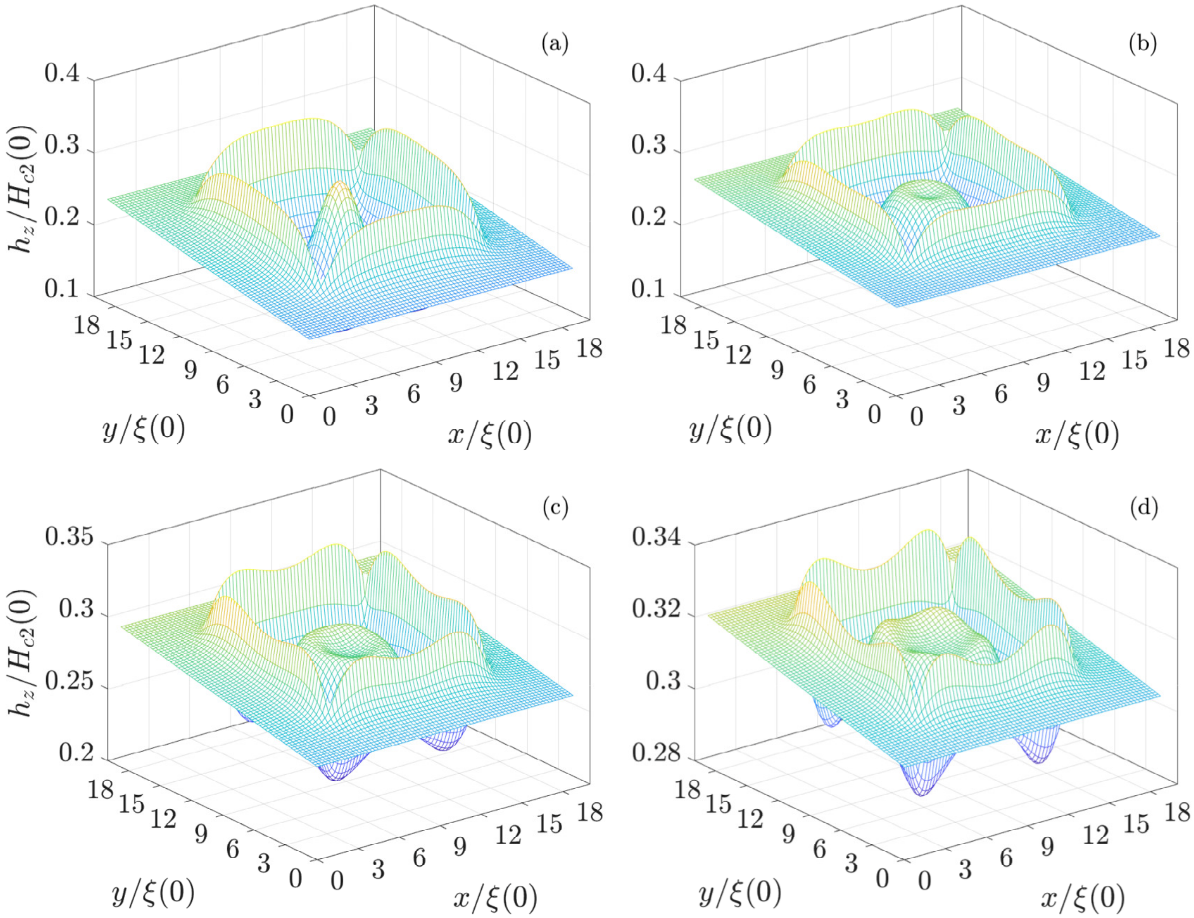

Figure 6. (Color online) Intensity of the z component of the local magnetic field for four values of the externally applied magnetic field for the same system described in Fig. 5.

4.2. Field-Cooled

We also investigated the vortex state for films of larger dimensions and found the vortex configurations for both the ZFC and the FC. We learned from this study that the FC approach produces many more configurations than the ZFC one. Systems that exhibit type I behaviour in the ZFC method present vortex formation even for smaller thicknesses in the FC context. Below, we show only states produced by the FC branch. In Fig. 8 we show four vortex states for a film of dimensions $20\xi(0) \times 20\xi(0) \times 0.7\xi(0)$ and temperature $\tau = 0.85$. For high magnetic fields, the vorticity is large. Thus, the vortices are so dense that it is necessary to take the magnitude of ψ at a logarithmic scale to visualize the vortex cores. As we can see, vorticity decays with decreasing the applied field, with the vortex configuration presenting giant vortices in some cases (panels (b), (d), and (f)). We note that, even with a low magnetic field applied, when the shielding currents are small, the vortices do not spread over the sample, which suggests a non-monotonic vortex-vortex interaction involving short-range repulsion and long-range

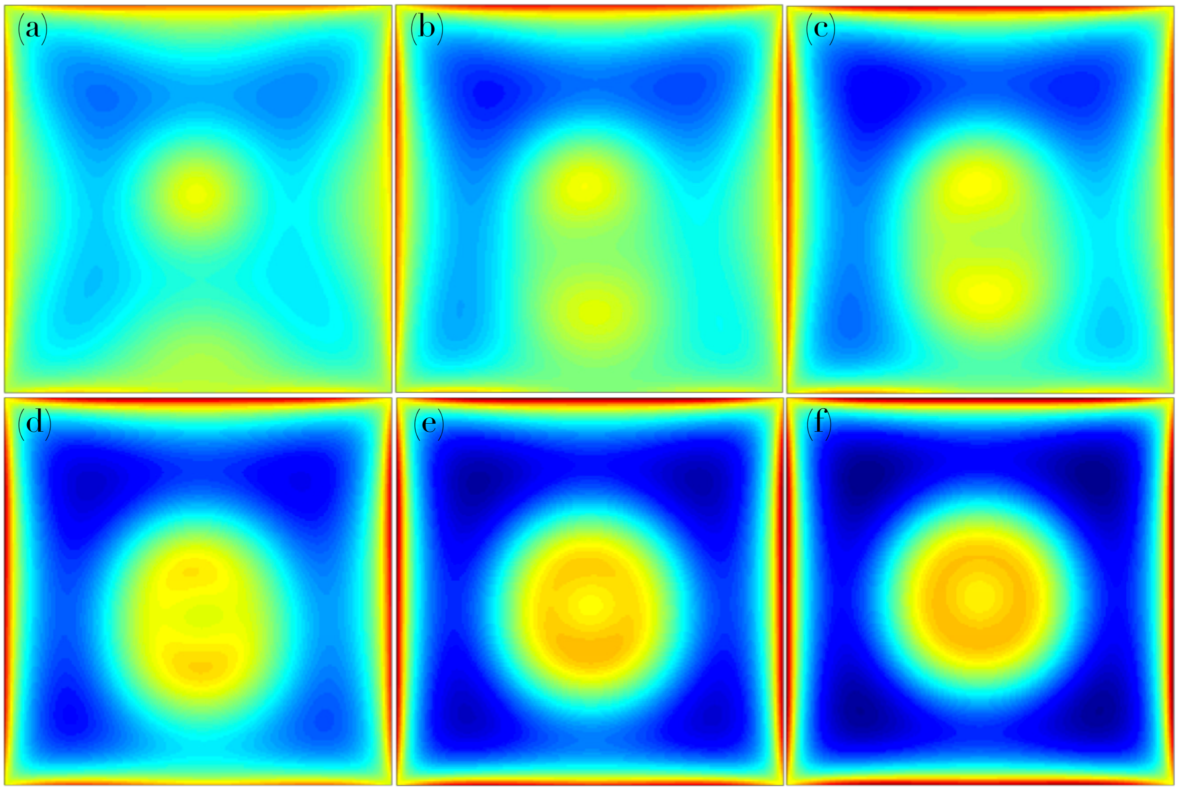

Figure 7. (Color online) Metastable vortex states for the applied field $H = 0.247H_{c2}(0)$. Panels (a) to (f) present the evolution of the local magnetic field profile from the nucleation of the second vortex to the formation of the giant vortex in a ring-like pattern.

attraction. The influence of several parameters makes it difficult to fully describe the vortices' interactions, but our results do make clear that they are not always repulsive, as in a conventional type II superconductor.

5. Conclusions

In summary, by numerically solving the 3D TDGL equations for the case of mesoscopic thin-film superconductors, we were able to obtain the relation between the thickness d of the film and the κ_c below which the system presents no vortex formation, behaving as a type I superconductor. We found that the κ_c for a given thickness increases with temperature. We also studied the effect of the sample dimension on the κ_c curve, finding that an increase in the dimensions perpendicular to the applied field, with the sample still being mesoscopic, leads to a decrease in the analysed curve, which is related to the current distribution over the sample.

Finally, the vortex configurations were studied for several parameters, using two different procedures. In the ZFC procedure, we followed the evolution of the vortex patterns with an increasing magnetic field applied. In the FC procedure, we studied the evolution of the vortex patterns with a decreasing magnetic field applied. In both cases, we found a novel giant vortex configuration that presents a local minimum of the magnetic field at the centre of the vortex.

Acknowledgments

The authors thank the following Brazilian agencies for financial support: the São Paulo Research Foundation (FAPESP) (grant number 12/04388-0), the Coordenação de Aperfeiçoamento de Pessoal de Nível Superior - Brasil (CAPES) - Finance Code 001, and the National Council of Scientific and Technological Development (CNPq, grant 302564/2018-7). LRC thanks VUNESP for financial support in the form of a scholarship.

Contributions: ES conceived the work; LRC and TC carried out the theoretical analysis and the numerical simulations; LRC, ES, and RZ wrote the manuscript, with contributions from TC.

References

[1] Tinkham M 1963 *Physical Review* **129** 2413
[2] Pearl J 1964 *Applied Physics Letters* **5** 65–66
[3] Abrikosov A A 1957 *Soviet Physics JETP* **5** 1174
[4] Maki K 1965 *Annals of Physics* **34** 363–376
[5] Lasher G 1967 *Physical Review* **154** 345
[6] Callaway D J E 1992 *Annals of Physics* **213** 166–181
[7] Schweigert V A, Peeters F M and Deo P S 1998 *Physical Review Letters* **81** 2783
[8] Shi L M, Zhang L F, Meng H, Zhao H W, Zha G Q and Zhou S P 2009 *Physical Review B* **79** 184518
[9] Berdiyorov G R, Milošević M V and Peeters F M 2006 *Physical Review Letters* **96** 207001
[10] Palonen H, Jäykkä J and Paturi P 2013 *Journal of Physics: Condensed Matter* **25** 385702
[11] Córdoba-Camacho W Y, da Silva R M, Vagov A, Shanenko A A and Aguiar J A 2016 *Physical Review B* **94** 054511
[12] Dantas D S 2017 *Emergent vortex behavior in superconductors and superfluids with single and multicomponent quantum condensates* PhD dissertation Universidade Federal do Ceará, Physics Department, Fortaleza, Brazil
[13] Ginzburg V I 1956 *Soviet Physics JETP* **3** 621
[14] Gropp W D, Kaper H G, Leaf G K, Levine D M, Palumbo M and Vinokur V M 1996 *Journal of Computational Physics* **123** 254 – 266 ISSN 0021-9991 URL `http://www.sciencedirect.com/science/article/pii/S0021999196900224`
[15] Barba-Ortega J, Sardella E and Aguiar J A 2015 *Physics Letters A* **379** 732 – 737 ISSN 0375-9601 URL `http://www.sciencedirect.com/science/article/pii/S0375960114012705`
[16] Wolf S, Vagov A, Shanenko A A, Axt V M and Aguiar J A 2017 *Physical Review B* **96** 144515
[17] Vagov A, Shanenko A A, Milošević M V, Axt V M, Vinokur V M, Aguiar J A and Peeters F M 2016 *Physical Review B* **93** 174503
[18] Baelus B J and Peeters F M 2002 *Phys. Rev. B* **65**(10) 104515 URL `https://link.aps.org/doi/10.1103/PhysRevB.65.104515`
[19] Ge J, Gutierrez J, Cuppens J and Moshchalkov V V 2013 *Phys. Rev. B.* **88** 174503

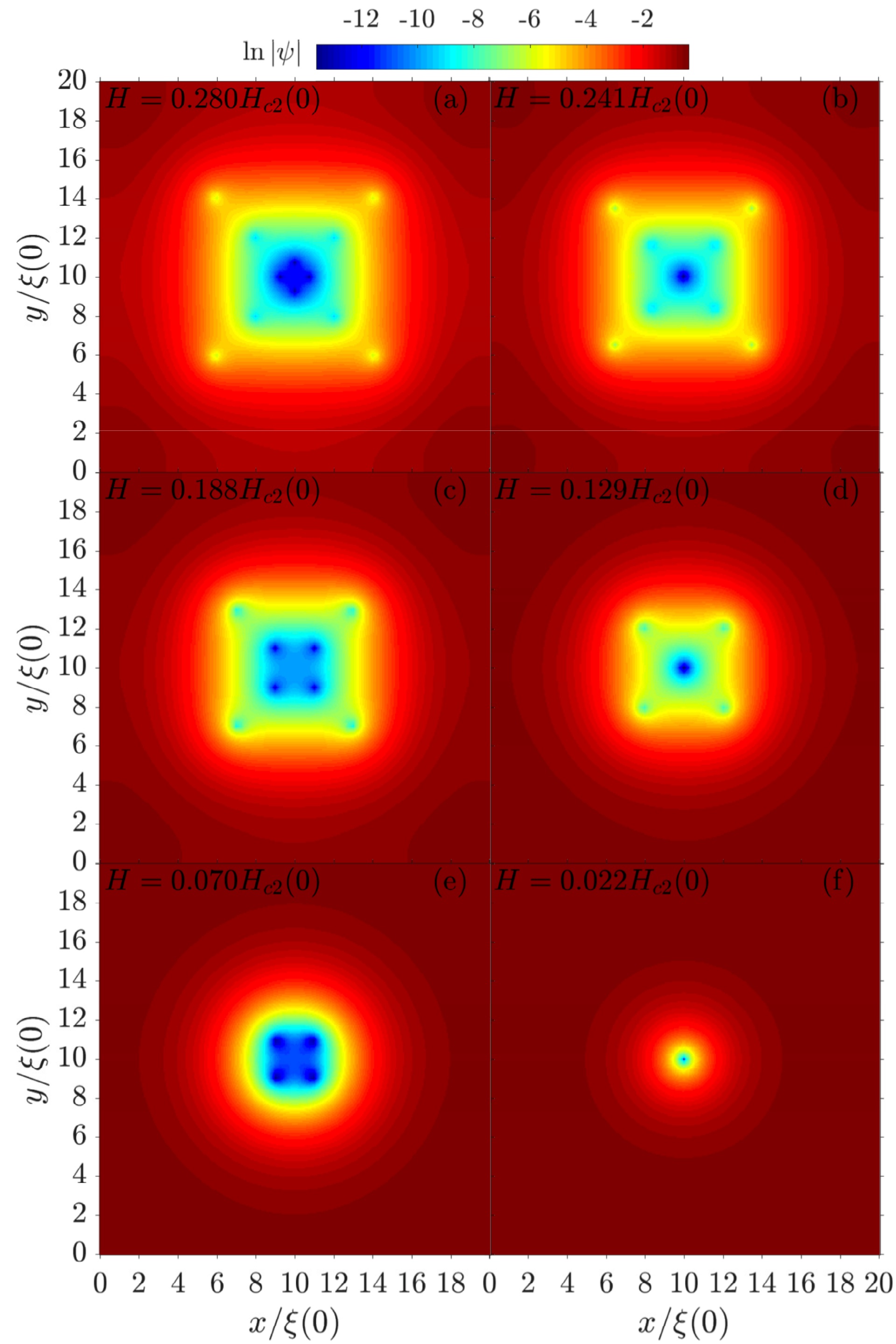

Figure 8. (Color online) Natural logarithm of the magnitude of the order parameter for four different values of applied magnetic field for the case of a superconducting thin film of dimensions $20\xi(0) \times 20\xi(0) \times 0.7\xi(0)$, $\kappa(0) = 0.32$ and $T = 0.85T_c$. (a)$L = 12$ single vortices; (b)$L = 10$ (eight single vortices and one giant vortex); (c)$L = 8$ single vortices; (d) $L = 6$ (four single vortices and one giant vortex); (e) $L = 4$ single vortices; (f) $L = 2$ (one giant vortex)

.